crystals

MDPI

Communication

A Study of Extended Defects in Surface Damaged Crystals

Claudio Ferrari [1,*], Corneliu Ghica [2] and Enzo Rotunno [1]

[1] IMEM Institute, National Research Council, 43124 Parma, Italy; enzo.rotunno@imem.cnr.it
[2] National Institute of Materials Physics, 077125 Magurele, Romania; cghica@infim.ro
* Correspondence: Claudio.Ferrari@imem.cnr.it; Tel.: +39-052-126-9223

Received: 7 November 2017; Accepted: 24 January 2018; Published: 30 January 2018

Abstract: We have analyzed by transmission electron microscopy silicon and GaAs crystals polished with sandpapers of different grain size. The surface damage induced a crystal permanent convex curvature with a radius of the order of a few meters. The curvature is due to a compressive strain generated in the damaged zone of the sample. Contrary to what was reported in the literature, the only defects detected by transmission electron microscopy were dislocations penetrating a few microns from the surface. Assuming the surface damage as a kind of continuous indentation, a simple model able to explain the observed compressive strain is given.

Keywords: curved crystals; surface damaged crystals; dislocation generation; crystal indentation

1. Introduction

Curved crystals may be used for the focalization of hard X- and gamma-rays through diffraction for gamma-ray astronomy [1], nuclear medicine [2], neutron beams conditioning [3], and X-ray microscopy [4]. According to X-ray diffraction theory, ideal mosaic crystals can achieve the maximum diffraction efficiency [5], intended as the integrated reflectivity of the diffraction profile. Nevertheless, the difficulty of obtaining the desired mosaic spread and mosaic structure makes the diffraction efficiency of real crystals much lower than that of ideal mosaic crystals.

A method for improving the diffraction efficiency is based on slightly bending the crystals. The curvature of lattice planes not only increases the angular interval of incident rays that are diffracted by the crystal but also enhances the diffracted peak intensity [6].

The application of a mechanical bending is not a practical method in optical systems where a large number of crystals is necessary. A possible method to produce curved crystals with permanent curvature without any external applied force is the controlled damaging of a crystal surface [7]. For instance, by surface damaging, bending with a uniform radius of curvature of 40 m of gallium arsenide, germanium, and silicon plates 2 mm in thickness could be achieved, as required for focusing gamma rays in a Laue lens for gamma ray astronomy [8,9].

Despite the empirical approach and the simplicity of the method, precise relationships have been found between the sandpaper grit size, the crystal thickness, and the induced curvature [10]:

- The curvature obtained is always convex, as seen from the damaged side of the crystal, and the same treatment induces curvatures depending on the orientation of the crystal surface and on the polarity of the crystal: a spherical curvature in (001)-oriented Si or Ge crystals and an elliptical curvature in (001)-oriented GaAs or InP crystals.
- The curvature $1/R$ is inversely proportional to the square of the sample thickness.

From these observations, it is clear that the curvature is induced by the formation of a compressive strained layer a few micrometers thick in the damaged zone [10]. To explain the formation of such a compressive strain after surface damage, different mechanisms have been proposed:

- the formation of an amorphous layer near the surface of the crystal generated by the relevant forces acting of the tips of the grains [11];
- the formation of cracks, which is the complete detachment of crystalline planes near the surface of the crystals [12,13]

To understand the formation of the compressive strain in the damaged zone, we analyzed by Transmission Electron Microscopy (TEM) several cross-sectional samples of treated crystals.

2. Experimental and Observation

2.1. Preparation of Crystals

Slices of different thicknesses of GaAs crystals grown by the liquid encapsulated Czochralski were cut from the ingots perpendicularly to the <100> growth direction, and the saw damaging was removed by a chemical etching with an HCl/HNO3 1:1 solution. Commercial GaAs samples were also used.

The surface damaging was obtained by means of a mechanical lapping process on one side of the planar samples. Two polishing machines were used: a Buehler Ecomec 4 (and a Buelher Vibromet 2 (Buehler, Uzwil, Zwizerland). Both are very versatile machines that allow one to produce different deformations by changing the grit of the sandpaper, the pressure per unit area applied on the samples, and the duration of the treatment. In the first machine, the samples were mounted on a plate with paraffin, and the plate was then positioned upside down facing the sandpaper plate. The two components rotate independently on two different axes so that the sample abrasion should be completely uniform on the entire surface of the sample plate. The sample assembling in the Vibromet 2 is similar, but in this case the sample holder is free to move on a vibrating plate covered with sandpaper. The samples were lapped for 10 min with P400 sandpapers, corresponding to an approximate grain size of 35 μm.

2.2. TEM Analysis

A TEM investigation has been conducted on a (001)-oriented GaAs sample, 500 μm thick, treated with a sandpaper P400 for 10 min which permitted to obtain a curvature radius R = 2.8 m.

The sample cross section, parallel to the (110) planes of the crystal, was mechanically polished down to ca. 300 μm. The resulting foils were ion-sputtered with a Gatan® DuoMill TM model 600 (Gatan, Pleasanton, CA, USA), to reach electron transparency. The final sample thickness was estimated to be between 70 and 120 nm, as evaluated by the extinction length of the electron beam in the GaAs lamella. A final gentle ion milling procedure was applied to the cross-section's thin lamella using a Gatan PIPS installation operated at a 3 kV accelerating voltage and 7° incidence angle.

A series of TEM micrographs recorded from neighboring areas are assembled in the panoramic image of Figure 1, which illustrates the effect of the treatment on the (001) surface, which is located on the right-hand side of the image. We did not observe defects such as cracks or inclusions in any of the observed samples but only short straight dislocation segments from the surface to ca. 3 μm in depth. We have no evidence of a formation of an amorphous phase near the surface of the sample as observed for instance in TEM specimens prepared by a focused ion beam [14,15], even if it is not possible to exclude the local formation of an amorphous layer a few nanometers thick during surface damage treatment.

The near-surface region shows a high defect density that extends for a few hundred nanometers. Below this first layer, the density of dislocations drastically decreases, and the dislocations, which appear as straight dark lines, can be observed singularly.

It is worth noting that two sets of dislocation lines can be identified in Figure 1b. The two sets are parallel to the (−111) and (1−11) planes, respectively, perpendicular to the (110) surface of the cross-section sample. Looking carefully at the dislocation segments, it appears that many dislocations cross the TEM sample, i.e., the dislocation lines are not parallel to the surface of the cross section.

Two families of parallel dislocations can be identified in Figure 1a,b. By comparing the micrograph in Figure 1b with the corresponding diffraction pattern in Figure 1c, it turns out that the habit planes of the two families of dislocations are (1−11) and (−111).

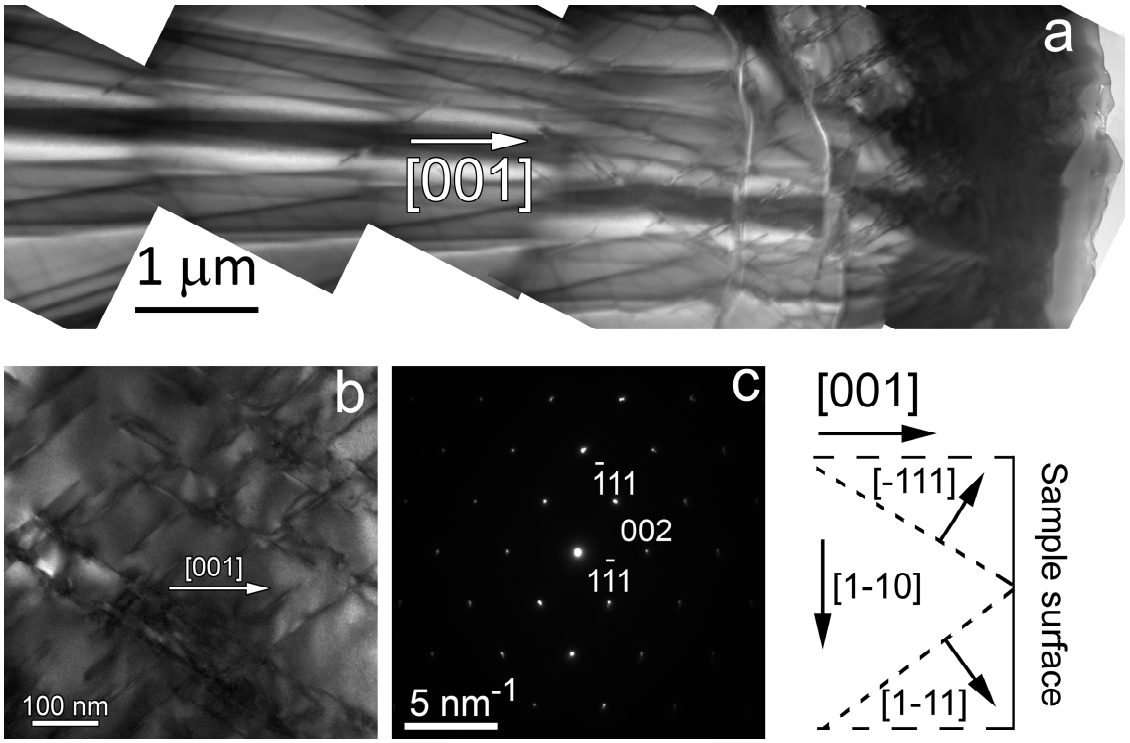

Figure 1. (**a**) Composed TEM image illustrating the material depth affected by the surface treatment and the density of dislocations along the first 7 µm below the surface. (**b**) TEM micrograph and the corresponding SAED pattern (c) in almost the [110] zone axis orientation from an area close to the wafer surface showing the formation of two families of dislocations included in the planes (−111) and (1−11).

By tilting the sample in such a way that only the (−111) and (1−11) reflections are excited, the two families of dislocations become respectively extinguished. It follows that, according to the $\vec{g} \cdot \vec{b} = 0$ invisibility criterion, the Burgers vectors of these dislocations are also parallel to the (−111) and (1−11) crystallographic planes, respectively.

Considering the dislocations with lines parallel to the (1−11) planes, based on the orientation-imaging conditions, it turns out that their Burgers vectors are parallel to the same planes. In the cubic structure of GaAs, an easy slip system is of the type {111}<110>, and the most common dislocations are perfect dislocations with Burgers vector a/2<110>. In the following analysis, we will assume only dislocations of this type. This may appear a critical limit of the model, but the assumption is justified by the fact that

- these dislocations have the lowest elastic energy among perfect dislocations in the face-centered-cubic (fcc) crystals;
- non-perfect dislocations are always associated to stacking faults increasing the elastic energy and limiting their mobility;
- these dislocations are typically observed in indented fcc crystals.

It follows that the Burgers vectors may have one of the following six values: a/2[110], a/2[011], a/2[−101], a/2[−1−10], a/2[0−1−1], and a/2[10−1], all of which are contained in the (1−11) plane.

A similar analysis is valid for the other set of dislocations with Burgers vectors lying in the (−111) habit plane. It follows that their Burgers vector may have one of the following six values: a/2[110], a/2[101], a/2[0−11], a/2[01−1], a/2[−1−10], and a/2[−10−1], all of which are contained in the (−111) plane.

The fact that the A and B dislocations are not extinguished simultaneously leads to the conclusion that the Burgers vector cannot be a/2[110] or a/2[−1−10]. In other words, the Burgers vector of the dislocations are not parallel to the electron beam and therefore not parallel to the wafer surface, the (001) plane. The Burgers vectors of the analyzed dislocations are one of the remaining four vectors—a/2[011], a/2[−101], a/2[0−1−1], or a/2[10−1] for the first set and a/2[101], a/2[0−11], a/2[01−1], or a/2[−10−1] for the second set. This means that all the Burgers vectors have a component $b^{||}$ parallel to the (001) surface of the processed wafer and a component $b^{\square}$ oriented perpendicular to the surface.

3. Model

To explain the compressive strain resulting from the surface grinding, we consider that the polishing by sandpaper behaves as a continuous indentation extended along the whole surface. Indentation in GaAs as in other fcc crystals results in the formation of rosettes made of dislocation loops gliding on (111) planes [16,17]. The sketch of the proposed mechanism is reported in Figure 2.

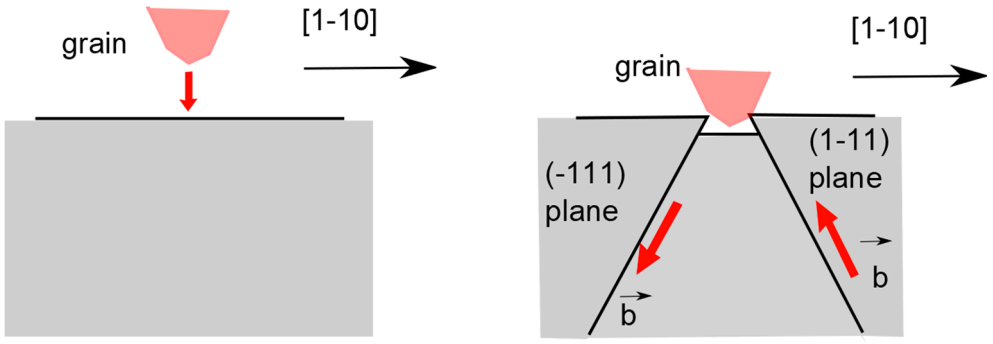

Figure 2. (**left**) Movement of the tip of a grain of the grinding paper in a direction perpendicular to the (001) surface of the crystal. (**right**) The indentation shifts part of the crystal below the original surface. The figure also shows the projection of the Burgers vector of the induced dislocations in the plane of the figure.

The indentation induces the glide of dislocations along the (1−11) planes for the set of dislocations on the right of the tip and along the (1−11) planes for the set on the left of the tip. In this illustration, we neglect for the sake of simplicity the set of dislocations that are also formed and glide on the (111) and (−1−11) planes inclined with respect to the plane of the figure. The Burgers vector components are deduced by the Burgers circuit. The Burgers vectors of the dislocations gliding on the (−111) and (1−11) planes must have opposite values of the Burgers vector component perpendicular to the surface and equivalent values of the Burgers vector component parallel to the crystal surface. According to Figure 3, the Burgers vector generated by the indentation should be

$$\vec{b_1} = \frac{a}{2}[\bar{1}0\bar{1}]\,\vec{b_2} = \frac{a}{2}[01\bar{1}] \tag{1}$$

for the (−111) glide plane and

$$\vec{b_3} = \frac{a}{2}[\bar{1}01]\,\vec{b_4} = \frac{a}{2}[011] \tag{2}$$

for the (1−11) plane. The identified Burgers vectors belong to the two sets deduced by extinction contrast in transmission electron micrographs, thus confirming the validity of the approach.

The Burgers vector have a common edge component parallel to the crystal surface, corresponding to the insertion of extra half planes form the surface of the crystal as shown in Figure 4. For a quantitative evaluation of the misfit induced by the dislocation glide, it is necessary to know the dimension of dislocation loops, a parameter not determined in the present study. A qualitative evaluation of the induced mismatch may be obtained by considering the density ρ of extra half planes as equivalent to the linear dislocation density ρ given by TEM observations. Based on Figure 1a,b, we may estimate $\rho \approx 10\ \mu m^{-1}$, leading to a misfit f value of the dislocated layer with respect to the unperturbed crystal:

$$f = \rho \cdot \frac{a}{2} \approx 8 \times 10^{-3}. \quad (3)$$

This results in a positive misfit of the damaged zone with respect to the part of the crystal free of dislocations, which induces a convex curvature to the crystal. Assuming a damaged layer thickness $t = 2\ \mu m$ and the misfit f value given by Equation (3) from the Stoney [18] equation, we obtain

$$R = \frac{T^3}{6ft(T-t)} \approx \frac{T^2}{6ft} = 2.6\ m \quad (4)$$

in which R is the curvature radius, T the crystal thickness, and f and t the misfit and thickness of the dislocated layer. Despite the rough approximation of the linear density of extra half planes, the result is in acceptable agreement with experimental data. The TEM analysis does not allow for the complete exclusion of the formation of an amorphous phase layer some nanometers thick at the top of the surface-treated samples. In principle, such a layer could contribute to the strain formation leading to a bending of the sample as described by Equation (4). Nevertheless, even by assuming a large mismatch between the amorphous phase and the underlying GaAs crystal, the effect of such a strained thin layer may be considered negligible with respect to the contribution originating from a 2-μm-thick dislocated layer.

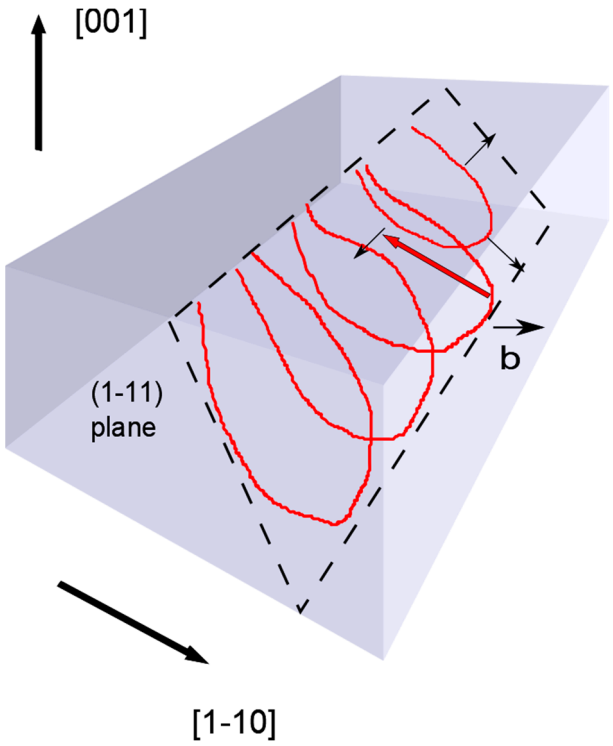

Figure 3. Loop formation and expansion due to surface damage and Burgers vector a/2[011] of a dislocation generated by indentation and gliding on the (1−11) plane.

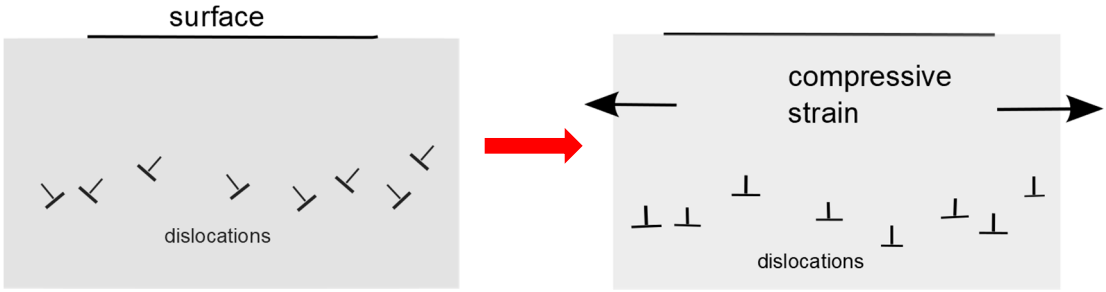

Figure 4. Sketch of the Burgers vectors of the dislocations generated by surface damaging. On the left, a randomly distributed Burgers vector is shown with a common component parallel to the surface. On the right, only the parallel component is shown. Each dislocation line corresponds to the insertion of extra half planes form the surface of the crystal, resulting in a compressive strain of the dislocated zone.

4. Conclusions

Crystals with a (001) surface damaged using sandpaper have been characterized by transmission electron microscopy in cross-sectional geometry. After the surface damaging, the samples exhibited a roughness comparable to the grit of sandpaper used, and a network of straight dislocation segments belonging to the (-111) and $(1-11)$ glide planes inclined to the (001) surface of the crystal extended to a depth of 3 μm, comparable to the dimension of the grains of the sandpaper. No other type of defects, such as cracks or inclusions were detected.

By changing the diffraction condition, the interpretation of extinction contrast permitted the establishment that the Burgers vector of the generated dislocation are parallel to the (-111) and $(1-11)$ glide planes.

A simple model for the formation of a compressive strain based on the dislocation glide in the damaged layer is given, in agreement with the measured sample convex curvature. Moreover, the elliptical curvature observed in surface-treated polar crystals such as GaAs and InP may be explained by the different glide velocity of dislocations on polar (111) glide planes.

We can conclude that the origin of sample curvature is the network of dislocations introduced by the damaging, considered as a continuous indentation of the crystal.

Acknowledgments: The authors acknowledge the CERIC-ERIC Consortium for the access to experimental facilities and financial support, under proposal number 20162066. CG acknowledges the financial support from the Project # PN16-480103 within the Core Program.

Author Contributions: C.F. and E.R. conceived and designed the experiments; C.G. performed the experiments; C.G. and E.R. analyzed the data; C.F. wrote the paper.

Conflicts of Interest: The authors declare no conflict of interest.

References

1. Ferrari, C.; Buffagni, E.; Bonnini, E.; Zappettini, A. X-ray diffraction efficiency of bent GaAs mosaic crystals for the LAUE project. *Proc. SPIE* **2013**, *88610D*. [CrossRef]
2. Roa, D.E.; Smither, R.K.; Zhang, X.; Nie, K.; Shie, Y.Y.; Ramsinghani, N.S.; Milone, N.; Kuo, J.V.; Redpath, J.L.; Al-Ghazi, M.S.A.L.; et al. Crystal diffraction lens for medical imaging. *Exp. Astron.* **2005**, *20*, 229. [CrossRef]
3. Courtois, P.; Bigault, T.; Andersen, K.H.; Baudin-Cavallo, J.; Ben Saıdane, K.; Berneron, M.; El-Aazzouzzi, A.; Gorny, D.; Graf, W.; Guiblain, T.; et al. Status and recent developments in diffractive neutron optics at the ILL. *Phys. B Condens. Matter* **2006**, *385*, 1271–1273. [CrossRef]
4. Borbély, A.; Kaysser-Pyzalla, A.R. X-ray diffraction microscopy: Emerging imaging techniques for nondestructive analysis of crystalline materials from the millimetre down to the nanometre scale. *J. Appl. Cryst.* **2013**, *46*, 295–296. [CrossRef]
5. Zachariasen, W.H. *Theory of X-ray Diffraction in Crystals*; Dover Pub. Inc.: New York, NY, USA, 1945.

6. Malgrange, C. X-ray Propagation in Distorted Crystals: From Dynamical to Kinematical Theory. *Cryst. Res. Technol.* **2002**, *37*, 654–662. [CrossRef]
7. Ferrari, C.; Buffagni, E.; Bonnini, E.; Korytar, D. High diffraction efficiency in crystals curved by surface damage. *J. Appl. Cryst.* **2013**, *46*, 1576–1581. [CrossRef]
8. Virgilli, E.; Frontera, F.; Rosati, P.; Bonnini, E.; Buffagni, E.; Ferrari, C.; Stephen, J.B.; Caroli, E.; Auricchio, N.; Basili, A.; et al. Focusing effect of bent GaAs crystals for γ-ray Laue lenses: Monte Carlo and experimental results. *Exp. Astron.* **2016**, *41*, 307–326. [CrossRef]
9. Liccardo, V.; Virgilli, E.; Frontera, F.; Valsan, V.; Buffagni, E.; Ferrari, C.; Bonnini, E.; Zappettini, A.; Guidi, V.; Bellucci, V.; et al. Study and characterization of bent crystals for Laue lenses. *Exp. Astron.* **2014**, *38*, 401–416. [CrossRef]
10. Buffagni, E.; Ferrari, C.; Rossi, F.; Marchini, L.; Zappettini, A. X-ray diffraction efficiency of bent GaAs mosaic crystals for the Laue project. *Opt. Eng.* **2014**, *53*, 047104.
11. Yan, J.; Asami, T.; Harada, H.; Kuriyagawa, T. Fundamental investigation of subsurface damage in single crystalline silicon caused by diamond machining. *Precis. Eng.* **2009**, *33*, 378–386. [CrossRef]
12. Davim, J.P.; Jackson, M.J. (Eds.) *Nano and Micromachining*; ISTE Ltd.: London, UK; John Wiley & Sons: Hoboken, NJ, USA, 2009; ISBN 978-1-84821-103-2.
13. Haapalinna, A.; Nevas, S.; Pähler, D. Rotational grinding of silicon wafers—Sub-surface damage inspection. *Mater. Sci. Eng. B* **2004**, *107*, 321–331. [CrossRef]
14. Holmström, E.; Kotakoski, J.; Lechner, L.; Kaiser, U.; Nordlund, K. Atomic-scale effects behind structural instabilities in Si lamellae during ion beam thinning. *AIP Adv.* **2012**, *2*. [CrossRef]
15. Korsunsky, A.M.; Guénolé, J.; Salvati, E.; Sui, T.; Mousavi, M.; Prakash, A.; Bitzek, E. Quantifying eigenstrain distributions induced by focused ion beam damage in silicon. *Mater. Lett.* **2016**, *185*, 47–49. [CrossRef]
16. White, J.E. X-ray Diffraction by Elastically Deformed Crystals. *J. Appl. Phys.* **1950**, *21*, 855. [CrossRef]
17. Bradby, J.E.; Williams, J.S.; Wong-Leung, J.; Swain, M.V.; Munroe, P. Mechanical deformation of InP and GaAs by spherical indentation. *Appl. Phys. Lett.* **2001**, *78*, 3235. [CrossRef]
18. Stoney, G.G. The Tension of Metallic Films Deposited by Electrolysis. *Proc. R. Soc.* **1909**, *82*, 172–175. [CrossRef]